Bio-inspired annelid robot: a dielectric elastomer actuated soft robot

2017 Bioinspir. Biomim. 12 025003

(http://iopscience.iop.org/1748-3190/12/2/025003)

IOP Publishing Bioinspir. Biomim. 12 (2017) 025003 doi:10.1088/1748-3190/aa50a5

Bioinspiration & Biomimetics

PAPER

Bio-inspired annelid robot: a dielectric elastomer actuated soft robot

RECEIVED
8 May 2016

REVISED
18 November 2016

ACCEPTED FOR PUBLICATION
29 November 2016

PUBLISHED
31 January 2017

Liang Xu[1,2,3], Han-Qing Chen[1,2,3], Jiang Zou[1], Wan-Ting Dong[2], Guo-Ying Gu[1,4], Li-Min Zhu[1] and Xiang-Yang Zhu[1]

[1] State Key Laboratory of Mechanical System and Vibration, School of Mechanical Engineering, Shanghai Jiao Tong University, Shanghai 200240, People's Republic of China
[2] University of Michigan-Shanghai Jiao Tong University Joint Institute, Shanghai Jiao Tong University, Shanghai 200240, People's Republic of China
[3] These authors contributed equally to this work.
[4] Author to whom any correspondence should be addressed.

E-mail: guguoying@sjtu.edu.cn

Keywords: soft robot, bio-inspired annelid robot, dielectric elastomer actuators, peristaltic locomotion

Supplementary material for this article is available online

Abstract

Biologically inspired robots with inherent softness and body compliance increasingly attract attention in the field of robotics. Aimed at solving existing problems with soft robots, regarding actuation technology and biological principles, this paper presents a soft bio-inspired annelid robot driven by dielectric elastomer actuators (DEAs) that can advance on flat rigid surfaces. The DEA, a kind of soft functional actuator, is designed and fabricated to mimic the axial elongation and differential friction of a single annelid body segment. Several (at least three) DEAs are connected together into a movable multi-segment robot. Bristles are attached at the bottom of some DEAs to achieve differential friction for imitating the setae of annelids. The annelid robot is controlled by periodic square waves, propagating from the posterior to the anterior, which imitate the peristaltic waves of annelids. Controlled by these waves, each DEA, one-by-one from tail to head, anchors to the ground by circumferential distention and pushes the front DEAs forward by axial elongation, enabling the robot to advance. Preliminary tests demonstrate that a 3-segment robot can reach an average speed of 5.3 mm s^{-1} (1.871 body lengths min^{-1}) on flat rigid surfaces and can functionally mimic the locomotion of annelids. Compared to the existing robots that imitate terrestrial annelids our annelid robot shows advantages in terms of speed and bionics.

1. Introduction

Since conventional rigid robots fail in a variety of unpredictable environments, typically in applications of search and rescue, industrial inspection, and medical endoscopy, robotic engineers incorporate soft technologies into their designs in order to enable robots to interact adaptively and flexibly with the environment [1–4].

One of the most commonly used soft technologies is shape memory alloy (SMA) [4–7]. Unfortunately, due to the thermo-mechanic actuation principle, i.e. deformation actuated by heating and cooling, SMA is neither energetically nor temporally efficient [8–10]. As a result, velocity of the SMA-based robots is limited.

Alternatively, dielectric elastomer (DE), a kind of electroactive polymer , is a promising soft actuation technology. The dielectric elastomer actuator (DEA) has its advantage in that its deformation is controlled by the electrostatic force directly generated by the most commonly used energy source, electricity, enduing it potentially shorter response time and higher energy efficiency. Typically, DEAs exhibit high actuation pressures (0.1–2 MPa), short response times (less than 1 ms) and high efficiencies (80%–90%) [11, 12].

The actuation principle of DEAs is straightforward. DE is a kind of smart material with high relative permittivity ε_r and low Young's modulus Y. As shown in figure 1(a), a thin layer of DE membrane with thickness d is sandwiched between two compliant electrodes. If a voltage V is applied across the two electrodes, the DE membrane compresses in thickness and stretches in plane, which is illustrated in figure 1(b).

The utilization of soft DE actuation technology in robotics is completely different from that of con-

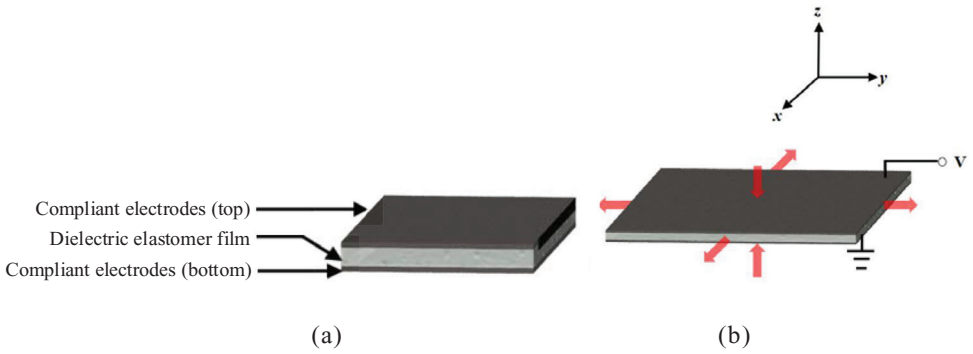

Figure 1. Actuation principle of a DEA with thin DE membrane sandwiched by two compliant electrodes. (a) Voltage off. (b) Voltage on.

ventional rigid locomotion schemes, which require innovations in locomotion strategies. Therefore, a growing number of biomimetic soft-bodied DE robotic systems inspired by natural animals have been reported [1–3, 13–22]. Works involving annelids are notably abundant [2, 3, 13–15]. The reason is that starting its evolution to terrestrial habitats as early as the Silurian, annelids possess one of the easiest body structures to move freely on dry land [23].

Annelids, different from vertebrates, possess hydrostatic skeletons, and thus adopt a characteristic peristaltic locomotion based on deformation [24]. The system of locomotion for a typical annelid includes the circular muscle, longitudinal muscle, and seta. Setae naturally hide beneath the cuticle, but can protrude and anchor to the ground in order to achieve differential friction during the body distention. Bodies of most annelids consist of practically identical segments. A separate circular muscle surrounds each segment, while the interior layer of longitudinal muscles runs from the anterior to the posterior [25]. Circular and longitudinal muscles form an agonist and antagonist muscle pair: when the circular muscle contracts circumferentially, it causes the movement of its corresponding segment so that it becomes longer and narrower; when the longitudinal muscle contracts axially, it opposes that movement by making the segments shorter and wider [25].

As a result, muscles enable annelid segments to perform two basic movements, the axial elongation to advance and the circumferential distention to anchor setae to the ground (figure 2) to achieve differential friction. Advancing the anterior segments, while anchoring the posterior ones, protrudes the head of an annelid. Retreating the posterior segments, while anchoring the anterior ones, stalls the head, but retrieves the tail. Figure 3 schematically shows the locomotion principle of annelids combining these two movements with a peristaltic wave (a periodic wave propagating from anterior to posterior) to take a stride forward. It is worth mentioning that the synchronicity of the circumferential distention and the axial elongation do not affect the efficiency of annelid locomotion if we reverse the direction of the peristaltic waves (figure 4).

Some available annelid robots are limited regarding locomotion efficiency, due to actuation technology (SMA in [4–6]), while others show incomprehensive imitation of the peristaltic locomotion (lack of differential friction in [13], which states that 'the circular muscle is just supplementary'). This motivated us to design and fabricate a new bio-inspired annelid robot based on DEAs with locomotion on flat rigid surfaces. We designed a 3D DEA that can move in two degrees of freedom (DOFs) to achieve axial elongation and differential friction, respectively, like annelid muscles. The annelid robot is fabricated based on the DEA and controlled by electric signals imitating the peristaltic waves of annelids. Experiments show that the prototype of our annelid robot can achieve the desired locomotion and speed performance on flat rigid surfaces and can perform locomotion similar to natural annelids.

2. Design and fabrication of DEAs

2.1. Design of DEAs

As described in the introduction, two essential traits, the axial elongation and the differential friction, are required in the actuator. Conventional DEAs fitting the model of figure 1 in a rigid frame, however, provide only a planar motion with one DOF, since the thickness distention cannot be utilized. A 3D structure is required to achieve the two abovementioned motions at the same time.

For this purpose, we use a DE minimum energy structure, in which a piece of pre-strained DE membrane is adhered to a piece of elastic frame (a piece of thin acrylic board frame specifically in our case) [26]. The restoring force of the DE membrane then bends the frame into a 3D minimum energy structure similar to figure 5(a). The structure is approximately a saddle surface.

When activated, the DE membrane stretches in the saddle surface, elongating the DEA in the y-direction and compressing its height in the z-direction. The y-direction elongation is analogous to the axial elongation of an annelid segment. The z-direction height compression achieves differential friction with flat rigid

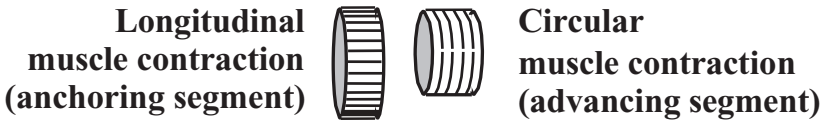

Figure 2. States of annelid segments during locomotion.

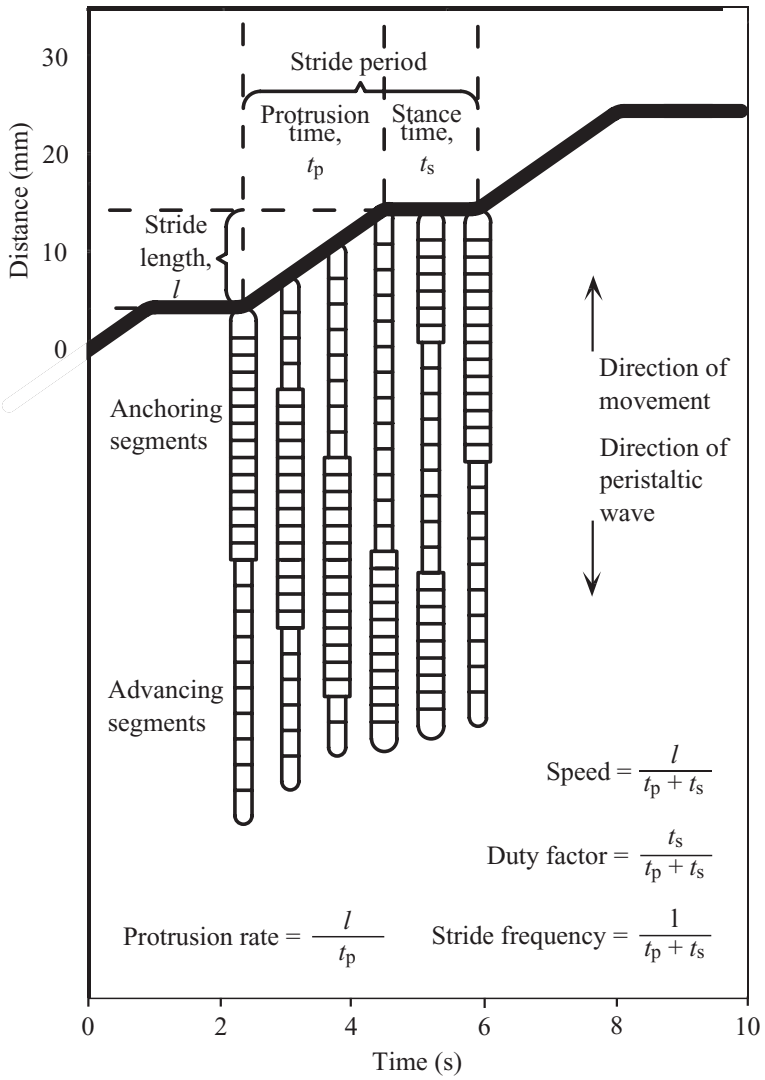

Figure 3. Process of peristaltic crawling by an annelid.

surfaces by lowering the bottom surface where the setae attach. Experimental results demonstrate that these two DOFs of motions are desirable at a DE membrane with a pre-strain percentage of 2.8 × 4.5.

To verify the abovementioned motion with two DOFs qualitatively, a laser displacement sensor is used. The experimental setup for verifying the axial elongation is shown in figures 6(a) and (b), while that for verifying the height compression is shown in figures 6(c) and (d). Note that in both experiments, since the DEA is an irregular surface, an opaque screen perpendicular to the displacement direction is introduced so that a laser displacement sensor can be accurately used. The DEA is tested on a rough surface, since the robot is designed to advance on such surfaces. A 2000 Vpp 0.5 Hz square wave with 2000 Vpp DC shift is applied to the DEA under test, and displacements associated with axial elongation and height compression are monitored by a laser displacement sensor.

The results of this experiment are clearly illustrated in figure 7. Displacement relating to axial elongation is the distance difference between the left and right leg tips of the DEA, and that relating to height compression is the distance difference from the bristle attaching point to the ground. The former is about 10 mm, and the latter is approximately 4 mm under 2000 V activation voltage. In real application, we can expect even larger displacements and shorter response time for the DEA, since the screen introduced here not only negatively affects the response but introduces a high oscillation frequency,

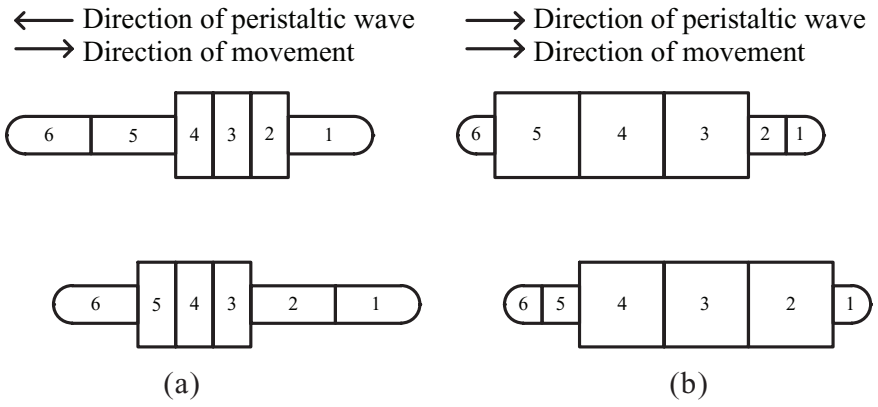

Figure 4. Equivalence of anti-synchronous and synchronous deformations in the locomotion of a 6-segment annelid. (a) Anti-synchronous distention and elongation. (b) Synchronous distention and elongation.

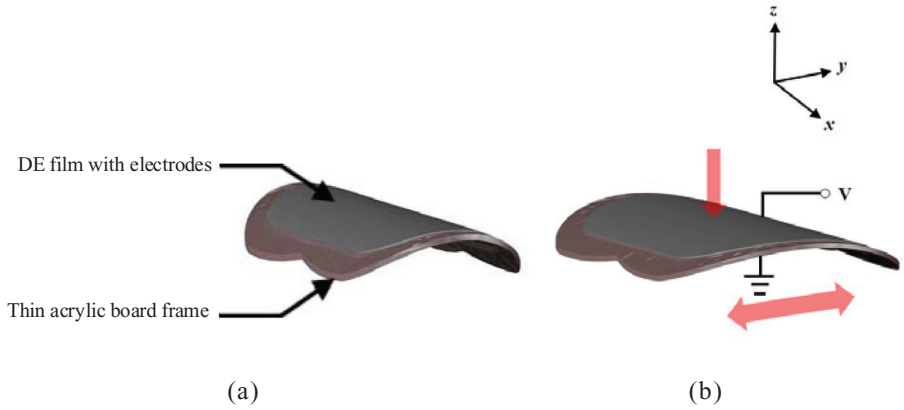

Figure 5. Pre-strained DEA bolstered by thin acrylic board frame. (a) Activated. (b) Deactivated.

which is visible in figure 7(a). Therefore, both the axial elongation and height compression are large enough for the locomotion of the annelid robot.

2.2. Fabrication of DEAs

According to the design, the structure of the DEA, from top to bottom, consists of a thin acrylic board frame, the top compliant electrode, the pre-strained DE membrane, and the bottom compliant electrode, as is illustrated in figure 8.

According to the test result of an experiment conducted to compare performances of several different DE materials, 3M's VHB 4910 acrylic elastomer gives the highest performance in terms of strain (215% relative area strain) and actuation pressure (up to 2 MPa) [8]. Therefore, we select VHB 4910 as the DE material for the actuator design of our biomimetic annelid robot. The glutinosity of VHB allows its direct adhesion to the thin acrylic board frame. A compliant electrode consists of an inner layer of carbon conductive grease (MG Chemical 846-80G) and an outer layer of protective silicone gel. Each of the silicone gel layers has a hole where copper wire (HornKing Jumper Wire 76555A724 1″x6Yds) is attached for connecting voltage.

The detailed procedure is as follows. A VHB 4910 membrane is first pre-strained with a stretcher shown in figure 9. A thin acrylic board frame is then adhered to the DE membrane. After that, carbon conductive grease and silicone gel are distributed uniformly on both sides of the DE membrane. Two copper wires are then attached on opposite sides for connecting voltage. Finally, the DEA is cut down carefully from the stretcher, and a fabricated DEA is shown in figure 10.

2.3. Selection of pre-strain percentage

For low strains, the thickness strain in the z-direction for the model in figure 1 can be approximated as [11]

$$s_z = -p_z/Y = -\varepsilon_r\varepsilon_0 E^2/Y = -\varepsilon_r\varepsilon_0 V^2/d^2 Y. \quad (1)$$

where ε_0 is the absolute permittivity, E is the magnitude of the electric field, and p_z is the stress induced by electric field in the z-direction.

As indicated by equation (1) and previous works on DE materials, larger pre-strain leads to a reduction in membrane thickness d, and therefore to a larger electrostatic pressure, for the same activation voltage [27]. Therefore, DE materials are usually pre-strained before fabricated into actuators. On the other hand, the material no longer satisfies the assumption of small strains and becomes stiffer (larger tangent modulus) at higher values of pre-strain percentage so that lower radial strains are obtained for the same electrostatic pressure, which

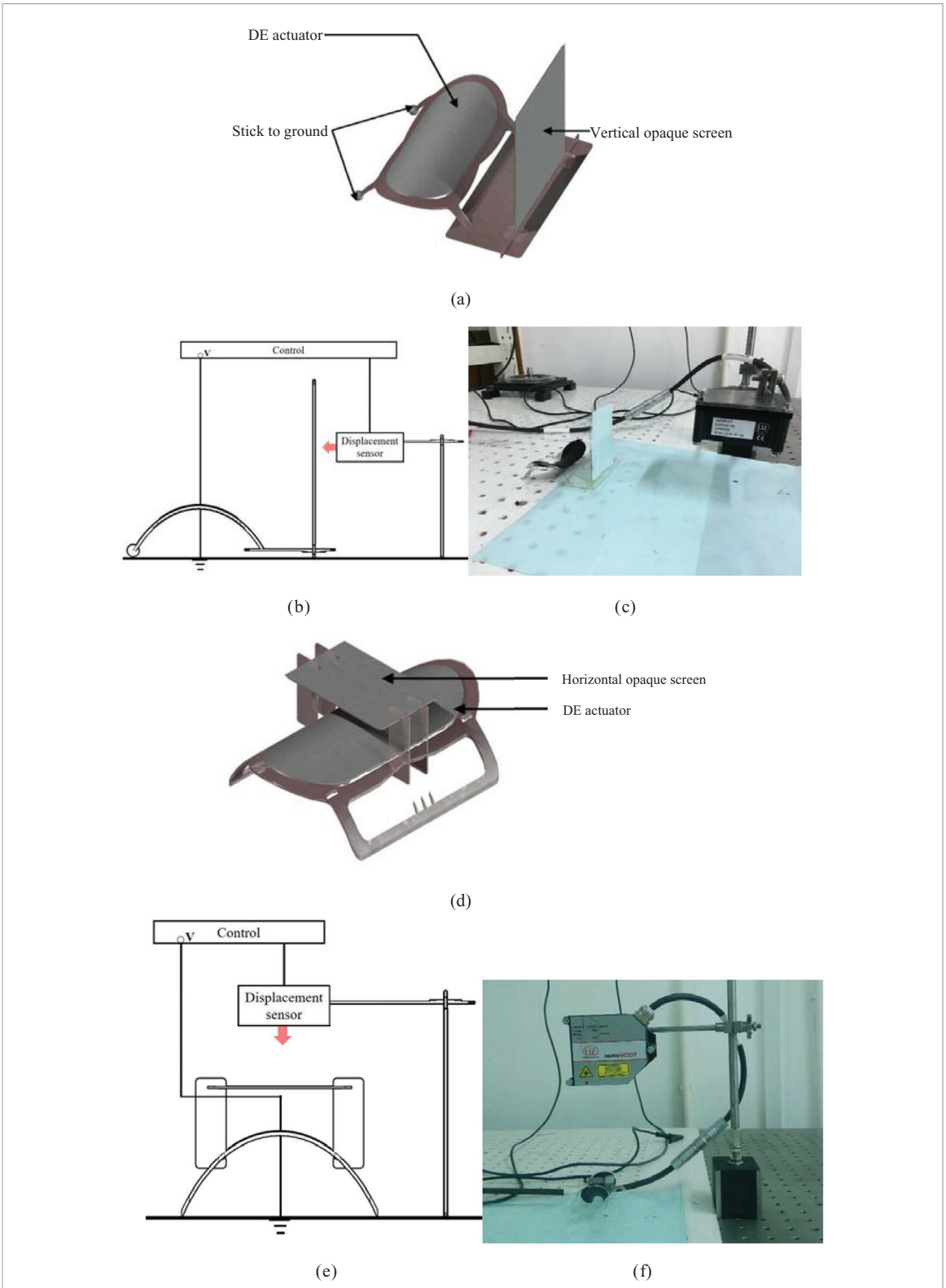

Figure 6. Experimental setups for qualitative verification of DEA function. (a)–(c) Axial elongation. (d)–(f) Height compression.

corresponds to the decrease of deformation [27, 28]. This brings about a tradeoff. As a result, experiments need to be conducted in to determine the optimal actuation voltage and pre-strain percentage.

We want to find a desirable pre-strain percentage of our DEA. In the experiment of section 2.1, a screen is required to make displacement sensors applicable, but it limits the motion of the actuator, so new setups need to be proposed. We resort to the technology of image processing. As is shown in figure 11, a camera is set to record the motions. The direction of the camera must be perpendicular to the plane of motion. References (graduated paper for axial elongation; 1 cm indicator pin, and base line for height compression) are also required to obtain the absolute values of displacements.

Four pre-strain percentages, 2.8×3.9, 2.8×4.1, 2.8×4.3, and 2.8×4.5 are tested for both axial elongation and height compression. The results are plotted in

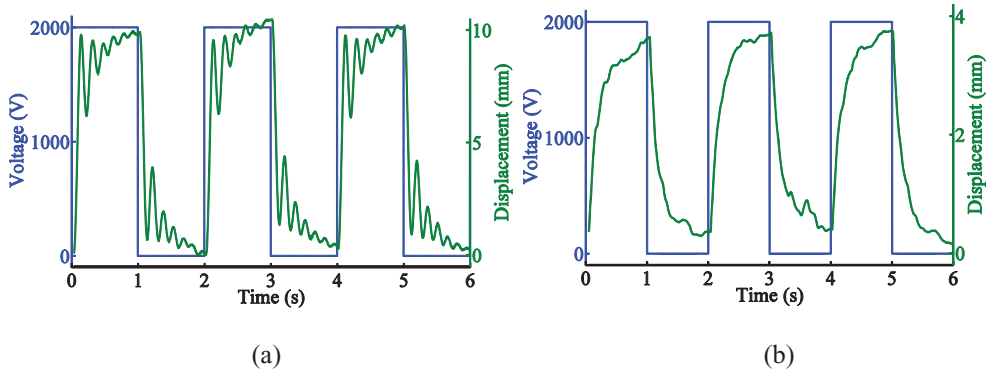

Figure 7. Experimental results for qualitative verification of DEA function. (a) Axial elongation. (b) Height compression.

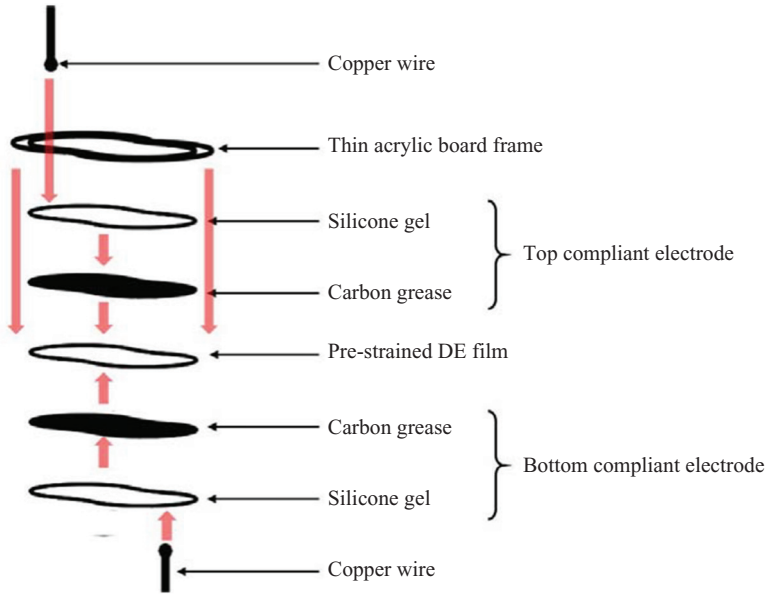

Figure 8. Exploded diagram illustrating each layer of the proposed DEA. DE film stretches when electric field is applied. Conductive carbon grease functions as compliant electrodes, which conducts electricity without limiting displacement. Silicone gel is used for protection. Copper wire extends the electrodes so that voltage can be applied.

figures 12(a) and (b) as displacement–voltage curves and in figures 12(c) and (d) as displacement–frequency curves with the dynamics of actuation high voltage supply shown in table 1. For all curves in figures 12(a) and (b), an approximate proportionality of displacement with a squared value of voltage can be realized, which is consistent with the trend indicated by equation (1). This means that all the pre-strain percentages applied for this robot are small enough to satisfy the condition of small strains, and little DE membrane stiffness occurs. DEAs with all four pre-strain percentages are tested with increasing actuation voltage until they break down. The pre-strain percentage 2.8×3.9 results in a breakdown voltage of 3100 V–3200 V, 2.8×4.1 results in 3200 V–3300 V, 2.8×4.3 results in 3300 V–3400 V, and 2.8×4.5 results in 3400 V–3500 V. For all curves in figures 12(c) and (d), the displacements in specified DOFs decrease with increasing actuation wave frequencies. This indicates that the DE minimum energy structure has a response time of more than 1 s. However, displacements can still be realized with a 6 Hz actuation square wave. The 4 mm axial elongation and 0.22 mm height compression for the percentage 2.8×4.5 at 6 Hz are still enough for the locomotion of the annelid robot, if well fabricated. Results show that the DEA with the pre-strained DE membrane of percentage 2.8×4.5 exhibits the largest displacement at high actuation voltages and high actuation frequencies and can achieve relatively high breakdown voltage for both axial elongation and height compression. Hence, it is desirable for the annelid robot.

Another experiment of actuation force is performed for the DEA with a pre-strain percentage of 2.8×4.5 with the same setup, since burden usually needs to be added so that more appreciable difference of friction can be achieved and the DEAs need to be connected together to push and pull each other to accomplish the locomotion. The result is shown in figures 12(e) and (f). Since the proposed annelid robot does not exceed 11 g in mass, burdens within 12 g are added to the DEAs so that a forced response of the DEAs can be obtained. As is shown in figures 12(e) and (f), displacements in

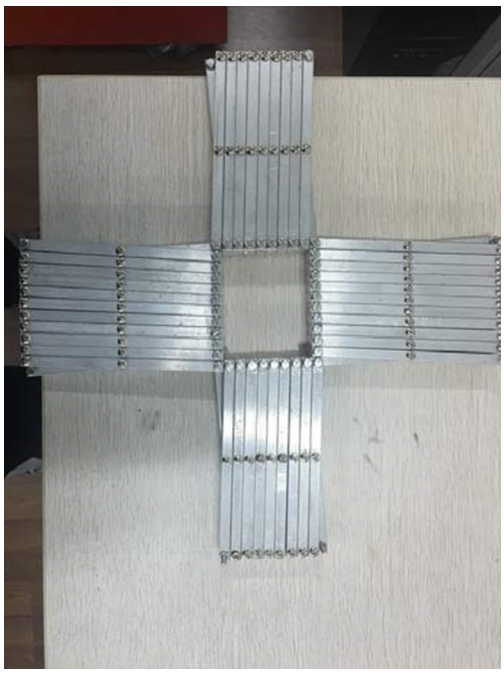

Figure 9. Stretcher used to pre-strain VHB 4910 membranes.

specified DOFs are still large with 8 g burden added and still enough with 12 g burden added.

3. Design of the annelid robot

3.1. Design of the annelid robot segments

The DEA proposed can perform two DOFs of motion, axial elongation and height compression inspired by the circular and longitudinal muscles of annelids. To make the DEA completely resemble a segment of an annelid robot, peripherals are required to imitate the function of setae.

During height compression, setae need to be anchored to the ground. We attach bristles at the bottom surface of the saddle-surfaced DEA to mimic setae so that the height compression of the DEA anchors them to the ground. Besides, setae need to hide beneath the cuticle in their natural state. We append acrylic board legs slightly longer than the bristles to the acrylic board frame to imitate the cuticle. Naturally, bristles do not touch the ground due to the height of the attached legs; when the DEA is activated, its height compresses so that the bristles protrude and anchor to the ground. Furthermore, to enhance the effect of differential friction accomplished by the setae, burdens may be placed on the DEA. In this way, the height compression of the DEA achieves differential friction on the bottom surface, which is sufficient for our purpose of locomotion on flat rigid surfaces (though this is still different from differential friction of the entire body circumference achieved by circumferential distention of natural annelids, which need to perform more complicated burying locomotion).

Consequently, the developed annelid robot segment is illustrated in figure 13, which is completely functional for locomotion on flat rigid surfaces in that it can alter friction by height compression and elongate axially (figure 14).

3.2. Assembly of the multi-segment robot

Since functional annelids are multi-segment (at least three segments), we need to connect the developed separate segments into a whole.

In annelids, longitudinal muscles run from the anterior to the posterior, connecting separate segments into a continuous entity. In our annelid robot, we introduce a DEA with no setae peripherals, but connection junctions (figure 15) to connect two adjacent segments. Such segments provide extra axial elongation to improve the locomotion ability of the entire annelid robot.

With the mechanism of connection seams and connection junctions, we integrate several functional segments into a multi-segment annelid robot, which is shown in figure 16. The shortest annelid possessing locomotive ability contains three segments, and it is used in the upcoming sections to explain the performance of our annelid robot (figure 17).

4. Locomotion performance

4.1. Control of the locomotion

The locomotion of the annelid robot requires delicate control of voltages applied to each segment. Considering the continuum deformation of actuators, the traditional control approaches are generally unavailable for control of the soft robots. In the literature, the commonly applied approach is to resort to biomimetic means.

Biologically, peristaltic wave controls the locomotion of multi-segment annelids. The proposed annelid robot segment has synchronous circumferential distention and axial elongation. According to figure 4, annelid robots constituted by such segments require peristaltic waves that direct from the posterior to the anterior.

One possible peristaltic wave for the locomotion of an n-segment annelid is shown in figure 18, which is a square wave with a period T propagating from segment n, the posterior segment, to segment 1, the anterior segment, delaying $T/2(n-1)$ for each segment.

4.2. Control system for peristaltic waves

To be activated, DEAs need high voltages (usually higher than 2 kV), which normal controllers fail to provide.

To solve the control problems, electric relays are introduced. Each developed DEA requires at least a single-pole double-throw relay (figure 19(a)) for control. The relay is controlled by 3 V from the dSPACE system connected to a computer (figure 19(b)). When the relay is activated, one electrode of the actuator is connected to the high DC voltage supply (figure 19(c)), and the other is connected to the ground. As a result, the DE membrane is charged and the actuator is

Figure 10. Completely fabricated DEA.

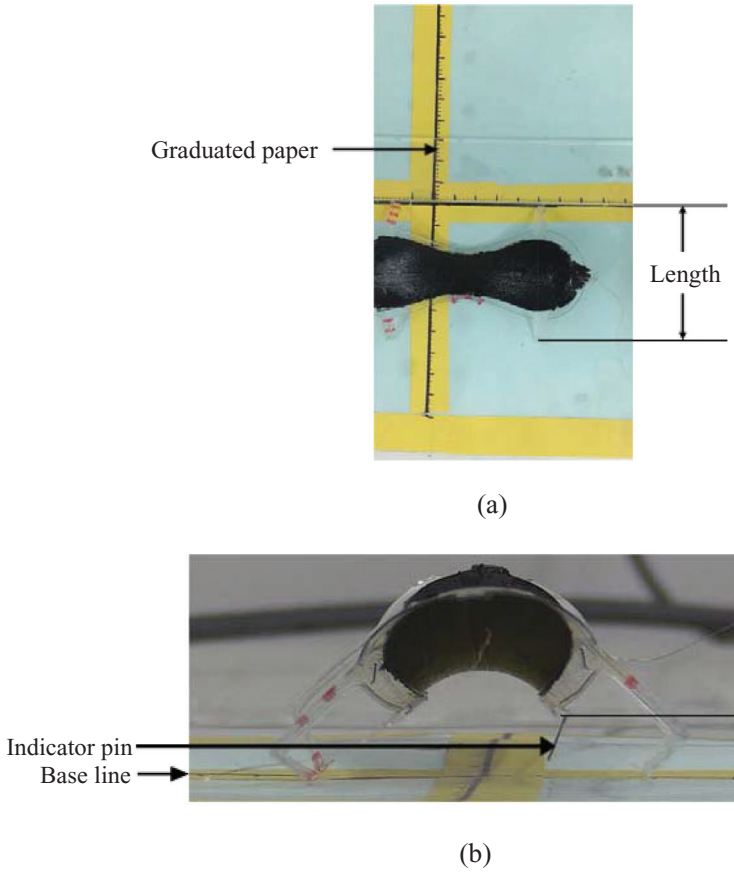

Figure 11. Experimental setups for finding optimum pre-strain percentage. (a) Axial elongation. (b) Height compression.

activated. When the relay is deactivated, both electrodes of the actuator are connected to the ground. As a result, the DE membrane is discharged and the actuator is deactivated.

Therefore, to control the 3-segment robot in figure 17, three single-pole double-throw relays are required (figure 20). In the circuit of figure 20, the dSPACE output $d1$ is 3 V, while both $d2$ and $d3$ are 0 V. As a result, segment 1 is activated, while both segments 2 and 3 are deactivated. To utilize this circuit to produce a desirable peristaltic wave, the output of dSPACE $d1$–$d3$ should be the signal in figure 21 with high voltage as 3 V and low voltage as 0 V, and the relays can magnify this signal to voltage higher than 2000 V with the help of the high DC voltage supply.

4.3. Performance of a 3-segment robot

To control a 3-segment annelid robot in figure 17, we design the peristaltic wave shown in figure 21. The low voltage is set to 0 V, and the high voltage is set to 3400 V for the stable performance of the DEAs. Since a segment needs to finish its response to a voltage change before

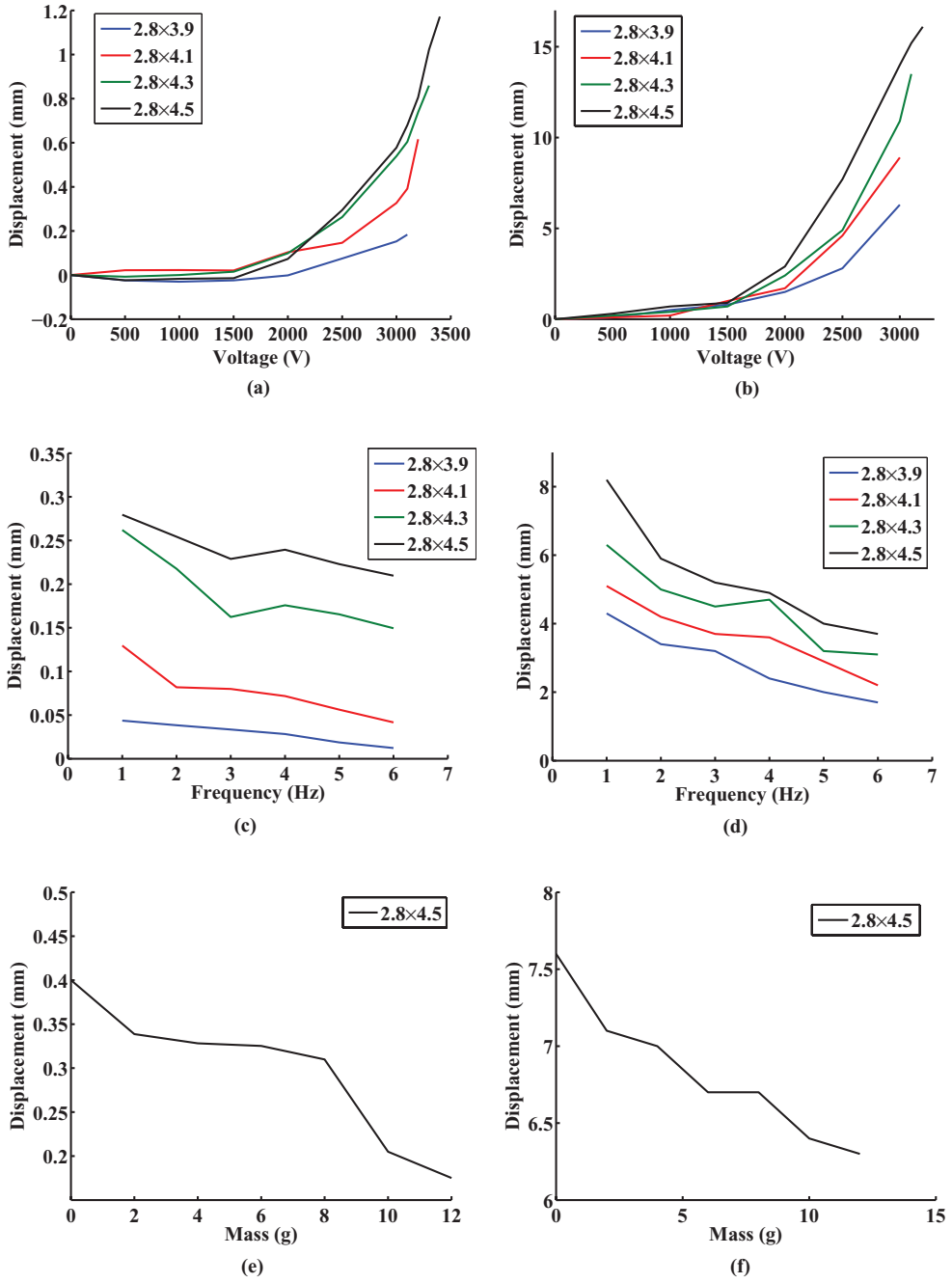

Figure 12. Experimental results for finding optimum pre-strain percentage. (a) Height compression with varying voltage. (b) Axial elongation with varying voltage. (c) Height compression with varying frequency. (d) Axial elongation with varying frequency. (e) Height compression with varying mass of burden. (f) Axial elongation with varying mass of burden.

Table 1. Dynamics of actuation high-voltage supply.

Experiments of	Waveform	Frequency (Hz)	Magnitude (V)	Burden (g)
Figures 13(a) and (b)	Step function	—	0–3400	0
Figures 13(c) and (d)	Square wave	1–6	3000	0
Figures 13(e) and (f)	Square wave	1	3000	0–12

the peristaltic wave propagates to the next segment, the period of the peristaltic wave T is set to 2 s, considering the typically 2 ms actuation time of DE materials.

By activating the annelid robot in figure 17 using the peristaltic wave in figure 21, we obtain the peristaltic locomotion of the robot illustrated in figure 22 and supplementary movie S1 (stacks.iop.org/BB/12/025003/mmedia). The 2 s motion illustrated is a stride period (motion of an annelid taken within a peristaltic wave period, figure 3), in which the first second is the protrusion time $t_p = 1$ s and the second is the stance time $t_s = 1$ s. The stride length l is 9 mm, which is reasonable given the approximately 3 mm axial elongation of each DEA at 3400 V. A parameter table is shown in table 2.

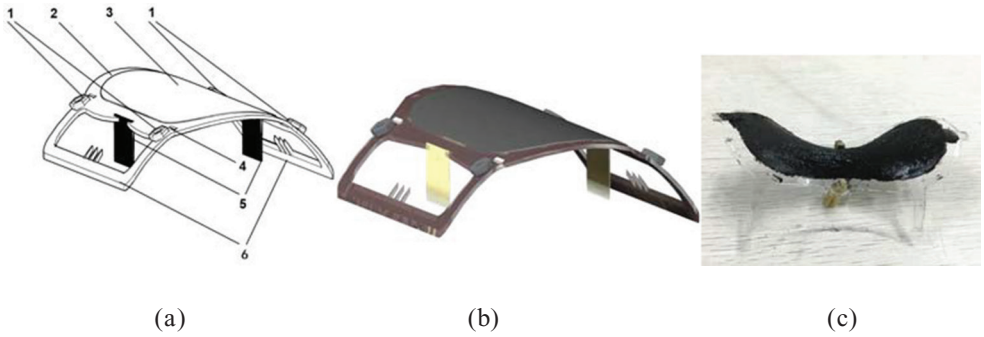

Figure 13. Design of functional biomimetic annelid segment. (a) Schematic diagram. (1) Burden (body mass). (2) Acrylic board frame. (3) DEA (muscles). (4) Connecting seam. (5) Bristle (seta). (6) Leg (cuticle). (b) Rendering diagram. (c) Photo of fabricated completely functional segment (without burden).

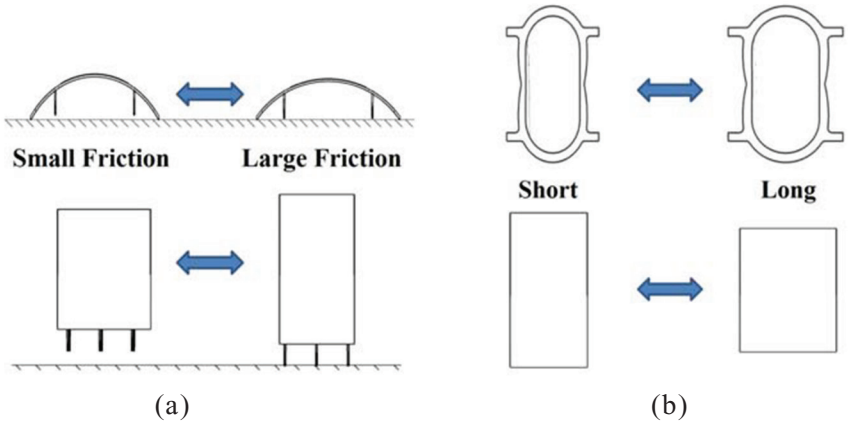

Figure 14. Functions of annelid robot segments are analogous to real annelid segments. (a) Circumferential deformation to alter friction (side view). (b) Axial elongation (top view).

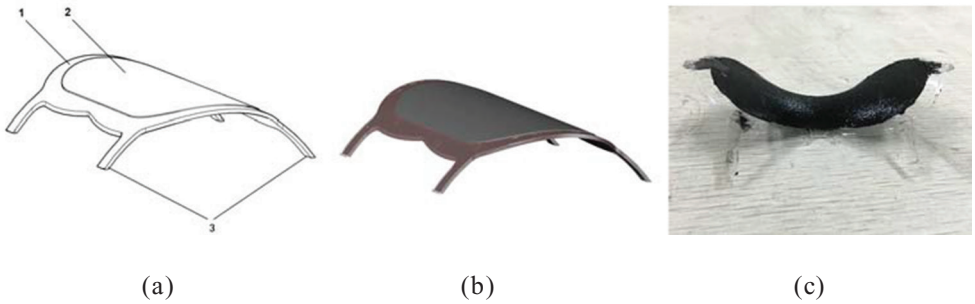

Figure 15. Design of connection segment. (a) Schematic diagram. (1) Acrylic board frame. (2) DEA (longitudinal muscle). (3) Connecting junction. (b) Rendering diagram. (c) Photo of fabricated connection segment.

Figure 16. A multi-segment annelid robot. (a) Rendering diagram. (b) Photo of fabricated robot.

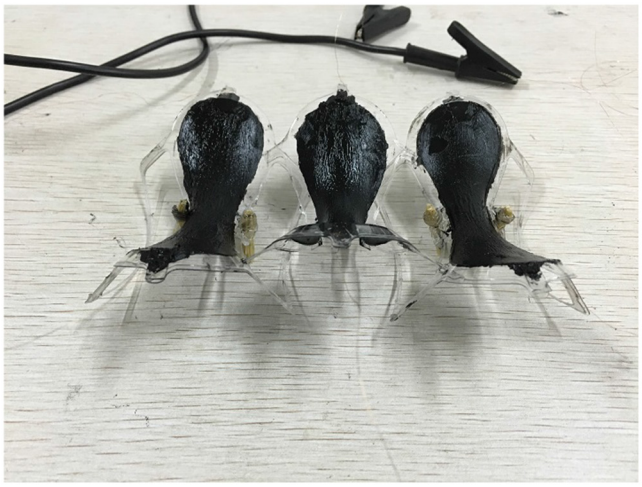

Figure 17. 3-segment annelid robot.

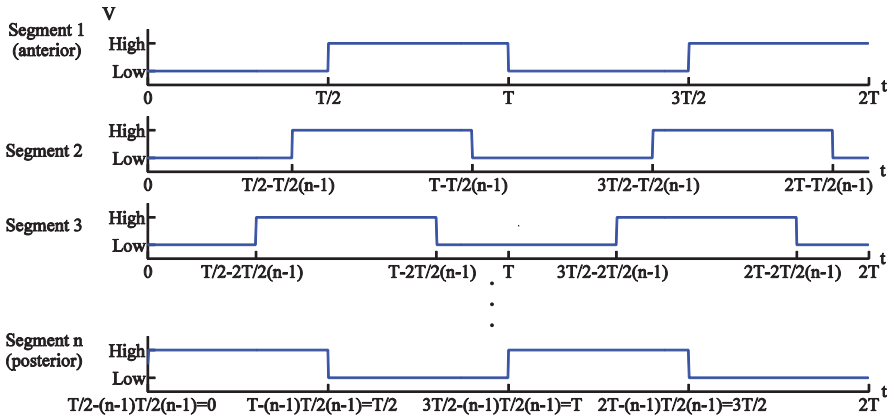

Figure 18. One possible peristaltic wave for the locomotion of an *n*-segment annelid.

This stride shown in figure 22 is a relatively fast one. In the long run, the average speed of the 3-segment annelid robot is 3.5 mm s^{-1}. Since the length of the robot is 17 cm, the average speed per unit length of the robot is about 1.233 body lengths min^{-1} or 4.12% of body length/cycle. The mass of the robot is 10.3 g, so the speed-mass ratio of the robot is about 20.39 mm $(min^{-1} \cdot g^{-1})$.

Another peristaltic control wave was used to test the locomotion performance. The same 3-segment annelid robot in figure 17 was controlled by a peristaltic wave shown in figure 21 with low voltage set to 0 V, the high voltage set to 2000 V, and period T set to 0.5 s. This time, the stride frequency is 2 Hz. The resultant peristaltic locomotion of the robot is shown in supplementary movie S2. In the long run, the average speed of the 3-segment annelid robot is 5.3 mm s^{-1}. Since the length of the robot is 17 cm, the average speed per unit length of the robot is about 1.871 body lengths min^{-1} or 1.56% of body length/cycle. The mass of the robot is 10.3 g, so the speed-mass ratio of the robot is about 30.87 mm $(min^{-1} \cdot g^{-1})$.

The 2 Hz actuated robot is faster than the 0.5 Hz actuated robot as expected, but the speed does not show proportionality to the actuation frequency, due to mainly two reasons. One reason is that as actuation frequency increases, the displacements in specified DOFs of motion decrease, as is shown in figures 12(c) and (d). As a result, the associated axial elongation decreases, and the differential friction has lower qualities, leading to a decrease in the stride length. Another reason is that a decreased displacement of height compression requires more accurate length of the bristles to achieve the same quality of differential friction, which is already beyond the extent of manual fabrication. As a result, there is slipping of the segments on the ground, which wastes part of the axial elongation. This second reason can be avoided by more accurate bulk manufacturing.

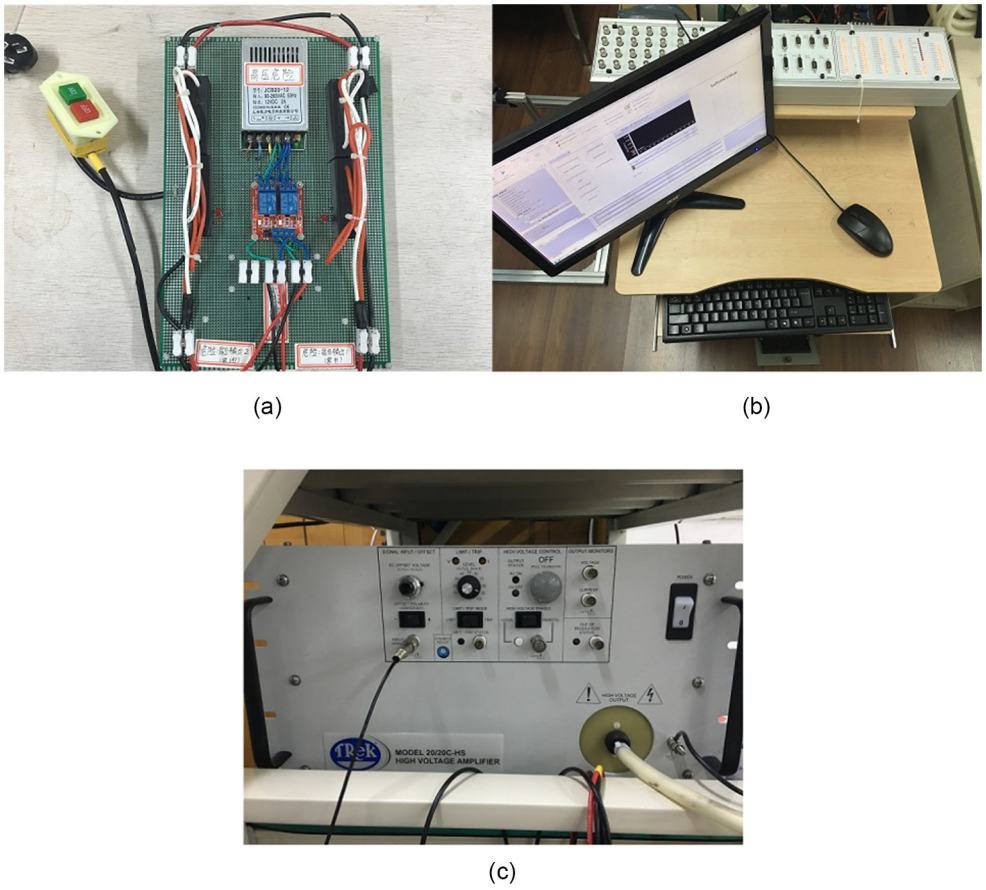

Figure 19. Devices for the control system for peristaltic waves. (a) Single-pole double-throw high-voltage relay (two of them). (b) dSPACE system connected to a computer. (c) High DC voltage supply.

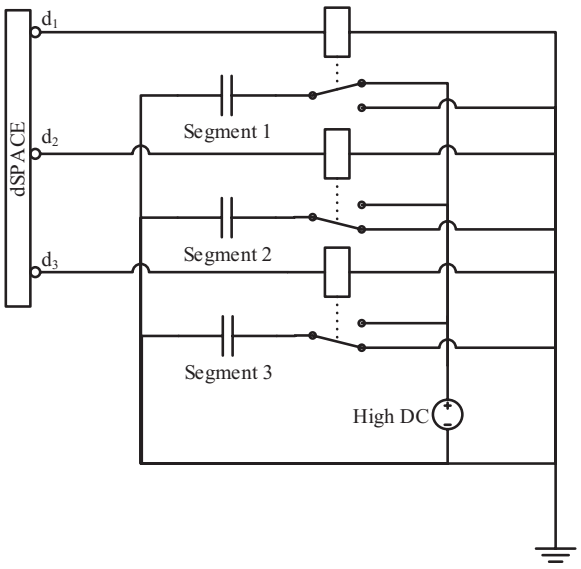

Figure 20. Electric circuit for the control system for peristaltic waves.

5. Discussion and conclusion

In this paper, we develop a soft robot bio-inspired by terrestrial annelids based on DEAs. By grasping the key point of annelid locomotion and key characteristic of DE materials, the developed robot is proved to have the desired locomotion, speed, and energy performance.

Our research has several advantages over existing robots inspired by terrestrial annelids. Table 3 shows a comparison of performance of the presented robot with that of other similar annelid robots.

(i) Our annelid robot imitates the locomotion of real terrestrial annelids accurately by grasping the key

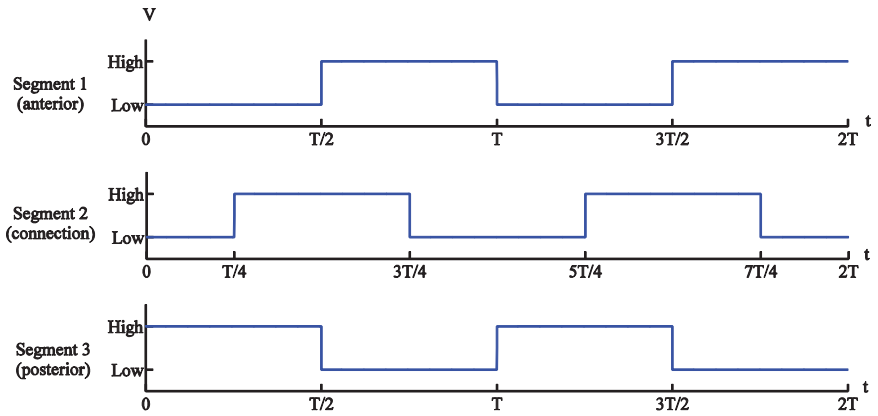

Figure 21. Peristaltic wave for activating a 3-segment annelid robot.

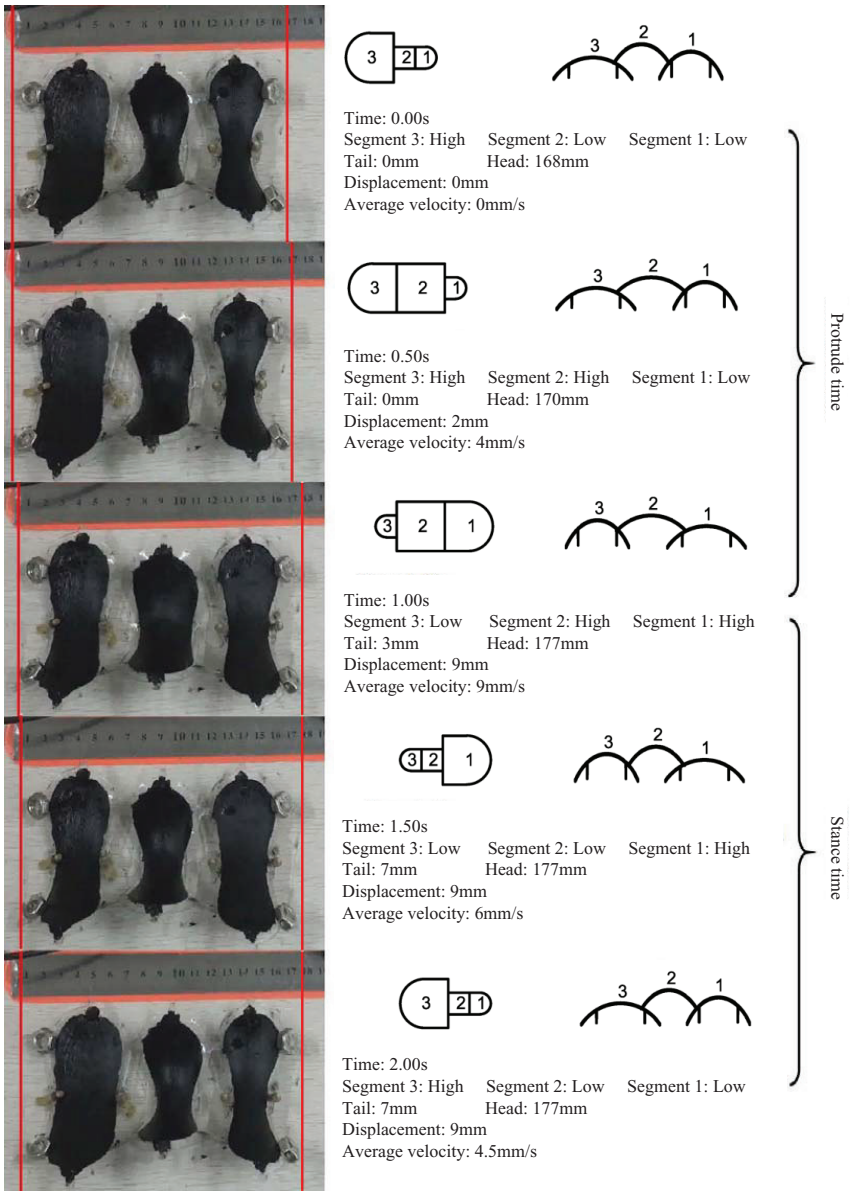

Figure 22. Graphical illustration of a stride taken by the annelid robot.

point of annelid locomotion, axial elongation, and differential friction. Some researches, however, leave out essential traits. Jung *et al* proposed an artificial annelid robot in their paper 'Artificial annelid robot driven by soft actuators' [13]. This robot also used DE as the material of

Table 2. Parameter table for the stride period shown in figure 22.

Parameter	Notation	Value
Stride period	T	2 s
Protrusion time	t_p	1 s
Stance time	t_s	1 s
Stride length	l	9 mm
Protrusion rate	l/t_p	9 mm s^{-1}
Stride frequency	$1/T$	0.5 Hz
Duty factor	t_s/T	0.5
Speed	l/T	4.5 mm s^{-1}

its actuator. However, they largely ignored the importance of differential friction, stating that 'the longitudinal muscle primarily contributes to the locomotion, but that of the circular muscle is just supplementary'. Consequently, the resulting robot advances with only 0.556% body lengths per cycle, indicating potential slipping that counteracts part of the axial elongation. Notably, their robot actually has a speed-length ratio of 3.333 body lengths per minute, which is better than ours, because they used a higher actuation frequency. Our robot still has some room to improve in terms of actuation frequency, which is now limited by the accuracy of the bristle length.

(ii) Our annelid robot uses DEAs instead of SMAs. This is significant, because DEAs exhibit higher actuation pressures (0.1–2 MPa), potentially shorter response times (less than 1 ms), and higher efficiencies (80%–90%). Menciassi *et al* fabricated a biomimetic robotic earthworm using soft actuators activated by SMAs [4]. They imitated the locomotion of annelids well by considering both the axial elongation and the differential friction. However, the response time of SMA actuators is long, and the maximum actuation frequency of their actuator is 0.6 Hz. Therefore, with normal differential friction mechanism, the speed was 0.44 body lengths per minute with a 0.47 Hz peristaltic wave for a 4-segment robot. Owing to the shorter response time of DEAs, our robot is faster and can be much faster by increasing the peristaltic frequency.

Compared with natural annelids, our annelid robot has already reached the range for natural annelids in terms of speed-length ratio. However, it is still inferior to natural annelids in terms of body length per cycle and speed-mass ratio. Improvements regarding the following three points are still required to enhance the locomotion performance and ensure that this work is scientifically rigorous.

(i) Locomotion can be improved with better differential friction mechanism, which limits the maximum actuation frequency that can be applied. Either a better manufacturing process of bristles or a new differential friction mechanism can be the solution. The former may be achieved by automated fabrication of both DEAs and bristles by delicately designed machines, which have the capability to ensure the accuracy of fabrication. The latter, however, may require some new bionic ideas. Menciassi *et al* [4] proposed an efficient mechanism of differential friction achieved by micro-legs 'fabricated by wire electro-discharge machining'. The result of this mechanism is that the speed of the robot is increased to about five body lengths per minute. Although this differential friction mechanism is different from annelids, (annelids achieve differential friction by a complementary DOF of motion of axial elongation generated by the same muscles) and more resembles the inchworm locomotion, it may be a potential solution to the actuation frequency limit of our robot.

(ii) The proposed DE minimum energy structure actuator is still unsatisfactory in terms of response time (more than 1 s, as is shown in experiments), which is another factor that limits the maximum peristaltic frequency. The response time is long, due to the acrylic board frame, which restricts the motion of the DEA, depriving part of its response capability. However, the frame is essential to form the DE minimum energy structure. Branz and Francesconi [29] studied this phenomenon in detail and introduced a feedback compensator that controls the device motion to achieve faster response of a DEA. The idea of feedback control is worth reference in our case and has the potential to improve the performance of the proposed annelid robot.

(iii) The problem of uncertainty analysis in soft material experiments should be addressed in future work even though it is very difficult, since uncertainty analysis is an important issue in a developed robot. Since the development of soft robots with the DEAs is still at an initial stage, this work, as well as other reported works [13, 20–22] on soft robots usually ignore such analysis. Even papers focusing on DE properties like the quoted [11, 27, 28] do not have uncertainty analysis. Of course, there are several reasons accounting for such difficulty. The first reason is that frequently used DE materials VHB4905 and VH4910 produced by 3M are designed for adhesion but not actuation. Hence, the variation in actuation properties of the resultant DE products is large, making the uncertainties of DEA experiments large. Besides, the fabrication process is usually manual, in which the pre-straining process can introduce significant uncertainty. Last, but not the least, graphic experimental setups are usually used in DEA measurements, which is the case in our experiment, and the system uncertainties of graphic experimental setups are usually large. These issues can be solved by proposing new production methods of DE materials

Table 3. Comparison of the presented robot with similar annelid robots.

Parameter	This work, 0.5 Hz	This work, 2 Hz	Jung *et al* [13]	Menciassi *et al* [4]	Natural annelids [24] (reference)
Width (mm)	120	120	20	10	—
Length (mm)	170	170	45	30	—
Mass (g)	10.3	10.3	>14.7	1.4	0.01–10
Actuation frequency (Hz)	0.5	2	10	0.47	0.1–0.5
Average speed (mm s^{-1})	3.5	5.3	2.5	0.22	—
Speed-length ratio (l min^{-1})	1.233	1.871	3.333	0.44	1.6–2.4
Body length/cycle (l/cycle)	4.12%	1.56%	0.556%	1.56%	5%–20%
Speed-mass ratio (mm ($min^{-1} \cdot g^{-1}$))	20.39	30.87	<10.20	9.43	>48

that can ensure the stability of DEA dynamics, automating the processes of DEA fabrication, and designing new experimental setups with lower systematic uncertainties. Research on the feasibility of uncertainty analysis on DEAs to improve scientific integrity will be necessary and challenging tasks for the further development of soft robots involving DEAs.

Acknowledgments

This work was in part supported by the National Natural Science Foundation of China under grant nos. 51622506 and 51620105002, and the Science and Technology Commission of Shanghai Municipality under grant 16JC1401000.

References

[1] Kim S, Laschi C and Trimmer B 2013 Soft robotics: a bioinspired evolution in robotics *Cell Press* **23** 287–94
[2] Mangan E V, Kingsley D A, Quinn R D and Chiel H J 2002 Development of a peristaltic endoscope *Proc. of IEEE Int. Conf. on Robotics and Automation* vol 1 pp 347–52
[3] Choi H R, Ryew S M, Jung K M, Kim H M, Jeon J W, Nam J D, Maeda R and Tanie K 2002 Microrobot actuated by soft actuators based on dielectric elastomer *Proc. of IEEE/RSJ Int. Conf. on Intelligent Robots and Systems* vol 2 pp 1730–5
[4] Menciassi A, Gorini S, Pernorio G, Liu W, Valvo F and Dario P 2004 Design fabrication and performances of a biomimetic robotic earthworm *Proc. of IEEE Int. Conf. on Robotics and Biomimetics* pp 274–8
[5] Kim B K, Lee M G, Lee Y P, Kim Y I and Lee G H 2006 An earthworm-like micro robot using shape memory alloy actuator *Sensors Actuators* **125** 429–37
[6] Yan G, Wang K and Shi J 2005 Research on micro robot for colonoscopy *Proc. of IEEE Engineering in Medicine and Biology 27th Annual Conf.* pp 1–4
[7] Seok S, Onal C, Wood R, Rus D and Kim S 2010 Peristaltic locomotion with antagonistic actuators in soft robotics *IEEE Int. Conf. on Robotics and Automation (ICRA)* (doi: 10.1109/ROBOT.2010.5509542)
[8] Cederstrom J and Humbeeck J V 1995 Relationship between shape memory material properties and applications *J. Phys.* III **5** C2-335–41
[9] Lara-Quintanilla A and Bersee H E 2016 A study on the contraction and cooling *J. Intell. Mater. Syst. Struct.* **27** 403–17
[10] Lara-Quintanilla A, Hulskamp A and Bersee H 2013 A high-rate shape memory alloy actuator for aerodynamic load control on wind turbines *J. Intell. Mater. Syst. Struct.* **24** 1834–45
[11] Pelrine R, Kornbluh R, Pei Q and Joseph J 2000 High-speed electrically actuated elastomers with strain greater than 100% *Science* **287** 836–9
[12] Park I S, Jung K, Kim D, Kim S M and Kim K J 2008 Physical principles of ionic polymer–metal composites *MRS Bull.* **33** 190–5
[13] Jung K M, Koo J C, Nam J D, Lee Y K and Choi H R 2007 Artificial annelid robot driven by soft actuators *Bioinspir. Biomim.* **2** S42–9
[14] Menciassi A and Dario P 2003 Bio-inspired solutions for locomotion in the gastrointestinal tract: background and perspectives *Phil. Trans. R. Soc.* **361** 2287–98
[15] Menciassi A, Spina G L and Dario P 2005 Polychaete-like undulatory robotic locomotion *Proc. of IEEE Int. Conf. on Robotics and Automation* pp 3029–34
[16] Safak K K and Adams G G 2002 Dynamic modeling and hydrodynamic performance of biomimetic underwater robot locomotion *Auton. Robots* **13** 223–40
[17] Godaba H, Li J S, Wang Y Z and Zhu J A 2016 Soft jellyfish robot driven by a dielectric elastomer actuator *IEEE Robot. Autom. Lett.* **1** 624–31
[18] Follador M, Tramacere F and Mazzolai B 2014 Dielectric elastomer actuators for octopus inspired suction cups *Bioinspir. Biomim.* **9** 1–10
[19] Shepherd R F, Ilievski F, Choia W, Morina S A, Stokesa A A, Mazzeoa A D, Xin C, Wanga M and Whitesides G M 2011 Multigait soft robot *Proc. Natl Acad. Sci.* **108** 20400–3
[20] Shian S, Bertoldi K and Clarke D R 2015 Use of aligned fibers to enhance the performance of dielectric elastomer inchworm robots *Proc. SPIE* **9430** 9430(1P)
[21] Conn A T, Hinitt A D and Wang P 2014 Soft segmented inchworm robot with dielectric elastomer muscles *Proc. SPIE* **9056** 9056(2L)
[22] Petralia M T and Wood R J 2010 Fabrication and analysis of dielectric-elastomer minimum-energy structures for highly-deformable soft robotic systems *IEEE/RSJ Int. Conf. on Intelligent Robots and Systems (IROS)* (doi: 10.1109/IROS.2010.5652506)
[23] Humphreys G S 2003 Evolution of terrestrial burrowing invertebrates *Advances in Regolith* I C Roach ed. (Canberra: CRC LEME) 211–5
[24] Kim J Q 1999 Kinematic scaling of locomotion by hydrostatic animals: ontogeny of peristaltic crawling by the earthworm lumbricus terrestris *J. Exp. Biol.* **202** 661–74
[25] Kim J Q 1998 Ontogenetic scaling of hydrostatic skeletons: geometric, static stress and dynamic stress scaling of the earthworm lumbricus terrestris *J. Exp. Biol.* **201** 1871–83
[26] Zhao J-W, Niu J-Y, McCoul D, Ge Y, Pei Q-B, Liu L-W and Leng J-S 2007 Improvement on output torque of dielectric elastomer minimum energy structures *Appl. Phys. Lett.* **107** 1–5
[27] Wissler M and Mazza E 2006 Mechanical behavior of an acrylic elastomer used in dielectric elastomer actuators *Sensors Actuators* A **134** 494–504
[28] Choi H R *et al* 2005 Effects of prestrain on behavior of dielectric elastomer actuator *Proc. SPIE* **5759** 283–91
[29] Branz F and Francesconi A 2016 Modelling and control of double-cone dielectric elastomer actuator *Smart Struct. Mater.* **9**